1,4-Diphosphabutadiyne: A Realistic Target for Synthesis? A Theoretical Investigation of C_2P_2, C_2N_2, [$Cr(CO)_5PCCP$], and [$(CO)_5Cr(PCCP)Cr(CO)_5$]

F. Matthias Bickelhaupt*[a] and Friedrich Bickelhaupt[b]

Abstract: To assess the viability of 1,4-diphosphabutadiyne (PCCP, **2a**) as a target for synthesis, we have investigated C_2P_2 isomers **2**, the end-on complexes [$Cr(CO)_5PCCP$] (**3**) and [$(CO)_5Cr(PCCP)Cr(CO)_5$] (**4**), as well as their side-on analogues **6** and **7**, respectively, using nonlocal density functional theory and a large, doubly polarized triple-ζ STO basis (BP86/TZ2P); C_2N_2 isomers **1** were included for comparison. The PCCP molecule **2a** turns out to be a thermodynamically stable, linear CP dimer with a 298 K carbon–carbon bond dissociation enthalpy (BDE) of 152.2 kcal mol^{-1}. The relatively high BDE and a C–C bond length of 1.336 Å, together with the results of a careful bond analysis, show that the PC–CP bond is best conceived as having partial triple bond character (i.e., P≡C–C≡P ↔ P–C≡C–P) similar to the NC–CN bond. However, the relatively low HOMO–LUMO gap of 2.5 eV in the π system of **2a** [versus 5.6 eV in NCCN (**1a**)] is indicative of a low kinetic stability: **2a** is likely to have a strong tendency toward polymerization. A conceivable strategy to protect and stabilize the evasive target molecule is coordination of the terminal P atoms to a transition metal fragment, for example, {$Cr(CO)_5$}. The (first) Cr–P bond dissociation enthalpy (for 298 K) in our model systems **3** and **4** amounts to 20 kcal mol^{-1}; side-on coordination (**6** and **7**) leads to an additional stabilization of about 1–2 kcal mol^{-1}. In a preliminary investigation, the effect of double side-on coordination of the P≡C bond of **2a** to {$Co_2(CO)_6$} was also briefly explored and found to furnish considerable stabilization. Furthermore, the differences in geometry (e.g., linear versus nonlinear) and bonding in CP and CN dimers are discussed and related to the electronic structures of the monomers. The bonding in the linear CC–NN and CC–PP codimers is also analyzed. We also address the question why flash vacuum thermolysis (FVT) of norbornadienonazine, although it does contain the CNNC unit, yields nearly exclusively CNCN (**1b**) and only a trace of CNNC (**1c**).

Keywords: coordination modes · density functional calculations · diphosphabutadiyne · orbital interactions · phosphorus

Introduction

There is a remarkable discrepancy in our knowledge about four-atom molecules C_2X_2 containing two carbon atoms and two atoms X of Group 15 such as C_2N_2 (**1**; X = N) and C_2P_2 (**2**; X = P). One representative, cyanogen (formally 1,4-diazabutadiyne, NCCN, **1a**), is stable under normal conditions; it was first prepared as early as 1815 by nobody less than Gay-Lussac[1] and has been intensively studied since.[2] In contrast, its positional linear isomers isocyanogen (CNCN, **1b**)[3, 4] and especially diisocyanogen (CNNC, **1c**)[5] are rather unstable, and it is therefore not surprising that their discovery was reported nearly two centuries later in 1988 and 1992, respectively.

N≡C–C≡N **1a** C≡N–C≡N **1b** C≡N–N≡C **1c**

P≡C–C≡P **2a** C≡P–C≡P **2b** C≡P–P≡C **2c**

Much less is known about the corresponding phosphorus compounds **2**. This may be considered to be a consequence of the Double Bond Rule,[6, 7] which states that double or multiple bonds are stable only between elements of the Second Period, whereas those between higher row elements are usually *kinetically* unstable. In the present context, this means that under normal conditions C≡X triple bonds are stable in the case of the cyanides R–C≡N, while their phosphorus analogues R–C≡P are stable only when protected by bulky substituents R.

Only three reports have appeared on the occurrence of **2**.[8] They all concern 1,4-diphosphabutadiyne (PCCP, **2a**), the phosphorus analogue of the stable cyanogen (**1a**); to our knowledge, the 1,3-diphospha isomer CPCP (**2b**) and the 2,3-diphospha isomer CPPC (**2c**) have not been described.

[a] Dr. F. M. Bickelhaupt
Fachbereich Chemie, Philipps-Universität Marburg,
Hans-Meerwein-Strasse, D-35032 Marburg (Germany)
Fax: (+49) 6421-28-2189
E-mail: bickel@chemie.uni-marburg.de

[b] Prof. F. Bickelhaupt
Scheikundig Laboratorium, Vrije Universiteit,
De Boelelaan 1083, NL-1081 HV Amsterdam (The Netherlands)

0947-6539/99/0501-0162 $ 17.50+.50/0 *Chem. Eur. J.* **1999**, *5*, No. 1

Compound **2a** was obtained by two different experimental approaches. In the first one, it was detected as a component of the equilibrium product mixture formed from the gaseous elements at temperatures above 2000 K; it was identified by mass spectrometry, and its atomization energy was determined as $D_0^\circ = 392.5 \pm 3.5$[8a] or 400.0 ± 7.0[8b] kcal mol^{-1}. In the second approach Bock and Bankmann[8c] attempted the synthesis of **2a** in a more rational fashion by dechlorination of $Cl_2P{-}C{\equiv}C{-}PCl_2$ on a heterogeneous catalyst at 670 °C, but again **2a** was formed as a minor product only and tentatively identified by photoelectron spectroscopy and mass spectrometry.

In the context of a program directed toward the development of synthetic strategies for alternative routes to **2a**,[9] we were interested in obtaining more information on the stability and viability of this compound through a detailed density functional theoretical (DFT) study (see Experimental Section).[10] In this context, the other two CP dimers (**2b** and **2c**) as well as the nitrogen analogues **1** were also of interest (Results and Discussion, section 1). We have tried to understand the differences in stability and geometry of these species through a detailed analysis and comparison of the electronic structure and bonding (Results and Discussion, section 2).[11]

Furthermore, the complexation behavior of **2a** was of interest because the unstable **1b** has been incorporated into the stable complex $[Cr(CO)_5CNCN]$,[12] and it is known that unsaturated phosphorus compounds can be similarly stabilized by coordination to transition metals.[7] It was therefore envisaged that the evasive **2a** might be isolable in the form of complexes such as $[Cr(CO)_5PCCP]$ (**3**) or $[(CO)_5Cr(PCCP)Cr(CO)_5]$ (**4**). In order to test this hypothesis, these two complexes were also incorporated in the present theoretical investigation, as well as some other coordination compounds derived from **2a** (Results and Discussion, section 3).

Abstract in German: *Um die Chancen für eine erfolgreiche Synthese von 1,4-Diphosphabutadiin (PCCP, **2a**) zu erkunden, haben wir die C_2P_2-Isomere **2**, die End-on-Komplexe $[Cr(CO)_5PCCP]$ (**3**) und $[(CO)_5Cr(PCCP)Cr(CO)_5]$ (**4**) sowie deren Side-on-Analoga **6** und **7** untersucht, wobei nichtlokale Dichtefunktionaltheorie angewendet sowie eine große, doppelt polarisierte Tripel-ζ-STO-basis (BP86/TZ2P) verwendet wurden; zum Vergleich wurden auch die C_2N_2-Isomere **1** berechnet. Das PCCP Molekül **2a** erweist sich als thermodynamisch stabiles, lineares CP-Dimer mit einer Kohlenstoff–Kohlenstoff-Bindungsdissoziationsenthalpie (BDE) von 152.2 kcal mol^{-1} bei 298 K. Die relativ hohe BDE und eine C–C-Bindungslänge von 1.336 Å sowie die Resultate einer detaillierten Bindungsanalyse zeigen, daß die PC–CP-Bindung am besten mit der Annahme eines partiellen Dreifachbindungscharakters verstanden werden kann ($P{\equiv}C{-}C{\equiv}P \leftrightarrow P{-}C{\equiv}C{-}P$), ähnlich der NC–CN-Bindung. Allerdings gibt die relativ kleine HOMO-LUMO-Lücke von 2.5 eV im π-System von **2a** (vgl. 5.6 eV in NCCN (**1a**)) einen Hinweis auf geringe kinetische Stabilität: **2a** neigt vermutlich stark zur Polymerisation. Eine aussichtsreiche Strategie zum Schutz und zur Stabilisierung dieses schwer zugänglichen Moleküls könnte die Koordination des terminalen Phosphoratoms an ein Übergangsmetallfragment wie $\{Cr(CO)_5\}$ sein. Die (erste) Cr–P-Bindungsdissoziationsenthalpie (bei 298 K) in unseren Modellsystemen **3** und **4** beträgt 20 kcal mol^{-1}; die Side-on-Koordination (**6** bzw. **7**) liefert eine zusätzliche Stabilisierung von ungefähr 1–2 kcal mol^{-1}. Der Effekt einer doppelten Side-on-Koordination der P≡C Bindung von **2a** an $\{Co_2(CO)_6\}$ wurde ebenfalls untersucht; sie führt zu einer erheblichen zusätzlichen Stabilisierung. Weiterhin werden Unterschiede in der Geometrie (z. B. linear/nichtlinear) und im Bindungsverhalten von CP- und CN-Dimeren diskutiert und mit der elektronischen Struktur der Monomere korreliert. Auch die Bindungssituation in den linearen CC–NN- und CC–PP-Co-Dimeren wird analysiert. Schließlich untersuchen wir noch das Problem, warum die Blitzvakuumthermolyse von Norbornadienonazin, obwohl es die CNNC-Teilstruktur bereits enthält, fast ausschließlich CNCN (**1b**) und nur eine Spur von CNNC (**1c**) liefert.*

Experimental Section

General procedure: All DFT calculations were performed using the Amsterdam-Density-Functional (ADF) program developed by Baerends and others.[4i, 13, 14] The molecular orbitals (MOs) were expanded in a large uncontracted set of Slater type orbitals (STOs) containing diffuse functions: TZ2P (no Gaussian basis functions are involved).[13c] The basis set is of triple-ζ quality, augmented with one set of 4p functions on Cr and Co, and two sets of polarization functions (3d and 4f) on C, N, and P. Core shells (1s for C and N; 1s, 2s, and 2p for P and Cr) were treated by the frozen-core approximation.[13a,b] An auxiliary set of s, p, d, f, and g STOs was used to fit the molecular density and to represent the Coulomb and exchange-correlation potentials accurately in each self-consistent field (SCF) cycle.[13a] The numerical integration was performed with the procedure developed by Boerrigter, te Velde, and Baerends.[13d]
Geometries were optimized using analytical gradient techniques.[13e] Frequencies[13f] were calculated by numerical differentiation of the analytical energy gradients. Energies, geometries, and frequencies were computed with the local-density approximation (LDA)[10a, 13g] with nonlocal corrections to exchange and correlation due to Becke[13h, 13i] and Perdew[13j] added self-consistently[13k] (BP86). Frequency calculations for **3** and **4** were performed with LDA only. Energies were calculated directly with respect to atoms in *one* numerical integration of the difference energy density $\varepsilon[\rho,\mathbf{r}] - \Sigma_A \varepsilon_A[\rho,\mathbf{r}]$ between the overall molecule and the constituent atoms [Eq. (1)].

$$\Delta E[\rho] = \int \varepsilon[\rho,\mathbf{r}] - \sum_A \varepsilon_A[\rho,\mathbf{r}]\mathrm{d}\mathbf{r} \quad (1)$$

In other words, we evaluate the energy of the overall molecule, $E[\rho] = \int\varepsilon[\rho,\mathbf{r}]\mathrm{d}\mathbf{r}$, and the energies of each of the component atoms, $E_A = \int\varepsilon_A[\rho,\mathbf{r}]\mathrm{d}\mathbf{r}$, in the same numerical integration grid. This provides more accurate relative energies than subtracting total energies from separate calculations, because the same relative numerical integration error applies to a much smaller quantity, yielding in turn a much smaller absolute error.

Bond analysis: The central electron-pair bond in the linear CN· and CP· dimers was analyzed using the extended transition state (ETS) method developed by Ziegler and Rauk.[14] The overall bond energy ΔE is divided in two major components [Eq. (2)].

$$\Delta E = \Delta E_{\mathrm{prep}} + \Delta E_{\mathrm{int}} \quad (2)$$

The preparation energy, ΔE_{prep}, is the amount of energy required to deform the separated fragments from their equilibrium structure to the geometry that they acquire in the composite molecule. The actual interaction energy, ΔE_{int}, between the prepared fragments can be further split up into three physically meaningful terms [Eq. (3)].

$$\Delta E_{\mathrm{int}} = \Delta V_{\mathrm{elst}} + \Delta E_{\mathrm{Pauli}} + \Delta E_{\mathrm{oi}} \quad (3)$$

Here, ΔE_{elst} corresponds to the classical electrostatic interaction between the unperturbed charge distributions of the prepared fragments and is usually attractive. The Pauli repulsion, ΔE_{Pauli}, comprises the four-electron destabilizing interactions between occupied orbitals and is responsible for any steric repulsion. The orbital interaction, ΔE_{oi}, accounts for electron-pair bonding,[14a] charge transfer (e.g., HOMO–LUMO interactions), and polarization (empty/occupied orbital mixing on one fragment due to the presence of another fragment).

Results and Discussion

1. C_2P_2 and C_2N_2: structures and energies: In this section we present the geometries and energies of a selection of C_2N_2 (**1**) and C_2P_2 (**2**) species obtained at the BP86/TZ2P level. They are summarized in Figures 1 and 2. For the assessment of the nature of our target molecule PCCP (**2a**), which has only been tentatively characterized experimentally,[8] it is helpful to compare this molecule with an existing analogue. Thus, let us first consider the well-known NCCN (**1a**) and its linear isomers in which phosphorus is replaced by its first-row congener nitrogen.

1.1. The C_2N_2 species: All three CN dimers **1a**–**1c** have stable minimum-energy structures of linear symmetry: $D_{\infty h}$ for **1a** and **1c**, $C_{\infty v}$ for **1b** (see Figure 1). An interesting phenomenon is that the central bond R_2 (see Scheme 1) becomes both shorter *and* weaker if one couples the two CN radicals through C–C (**1a**), N–C (**1b**), or N–N (**1c**) bonds: in this order, R_2 contracts from 1.373 to 1.305 to 1.274 Å, while the corresponding bond dissociation enthalpy (BDE $= -\Delta H$ at 298 K) decreases from 136.6 to 113.5 to 68.2 kcal mol^{-1}; the zero Kelvin electronic-bond dissociation energies, that is, $-\Delta E$, are 140.5 (**1a**), 117.2 (**1b**), and 71.4 kcal mol^{-1} (**1c**). The contraction of R_2 is due to the combined effect of the smaller effective size of nitrogen compared with carbon and to its higher electronegativity, which causes the weakly C–N antibonding cyanide SOMO to have a lower amplitude on nitrogen. These effects lead to an onset of both repulsive and bonding interactions at shorter bond lengths if N instead of C is involved in the central bond (for more details, see section 2 and ref. [4i]).

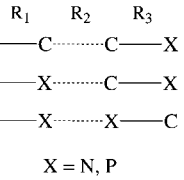

Scheme 1.

The C–N bond length of the isolated cyanide radical is 1.173 Å. It contracts by about 0.01 Å if cyanide binds through carbon to the another CN radical as in **1a** and **1b** (Figure 1). However, if CN binds through nitrogen, the terminal C–N bond expands by about 0.02 Å as in **1b** and **1c**.

There is yet another linear isomer, CCNN (**1d**), which can be conceived to be a codimer of C_2 and N_2 monomers, held together by a donor–acceptor bond between the valence state LUMO of C_2 (i.e., $3\sigma_g$) and the σ_{HOMO} of N_2 (again $3\sigma_g$). A more detailed discussion of this bond has been given by Scheller et al.[16] Compound **1d** is even higher in energy than the least stable CN dimer **1c**, although by 3.2 kcal mol^{-1} only. The C–C, C–N, and N–N bond lengths in **1d** are 1.277, 1.267, and 1.140 Å, respectively.

We have investigated the transformation of **1a** via TS(**1a**/**1b**) to **1b**, and of **1b** via TS(**1b**/**1c**) to **1c** (Figure 1). The 298 K activation enthalpies $\Delta H^{\neq}$ for these reactions are 57.6 and 80.4 kcal mol^{-1}, respectively. The reverse barriers are 34.5 (**1b** → **1a**) and 35.1 kcal mol^{-1} (**1c** → **1b**). Sunil et al.[4e] have reported two transition states for direct conversion of **1c** into **1a**, one of D_{2h} and the other of C_{2v} symmetry, which are 16.8 and 76.1 kcal mol^{-1}, respectively, above **1c** (ΔE at MP4/6-31G*//MP2/6-31G*). We have found similar structures **1e** and **1e′** at 23.2 and 65.4 kcal mol^{-1} above **1c** (ΔH_{298} at BP86/TZ2P; Figure 1). However, according to our vibrational analysis, these are actually transition states for the automerization of **1a** and **1c**, respectively, and *not* for the interconversion **1a** → **1c**. Likewise, in a recent computational study [B3LYP/6-311G(d)], Ding et al.[4l] were not able to find the transition states for the interconversion of **1c** to **1a** reported in reference.[4e] Instead, they located two different activated complexes that are, to some degree, structurally similar both to ours and to those of Sunil et al.,[4e] but

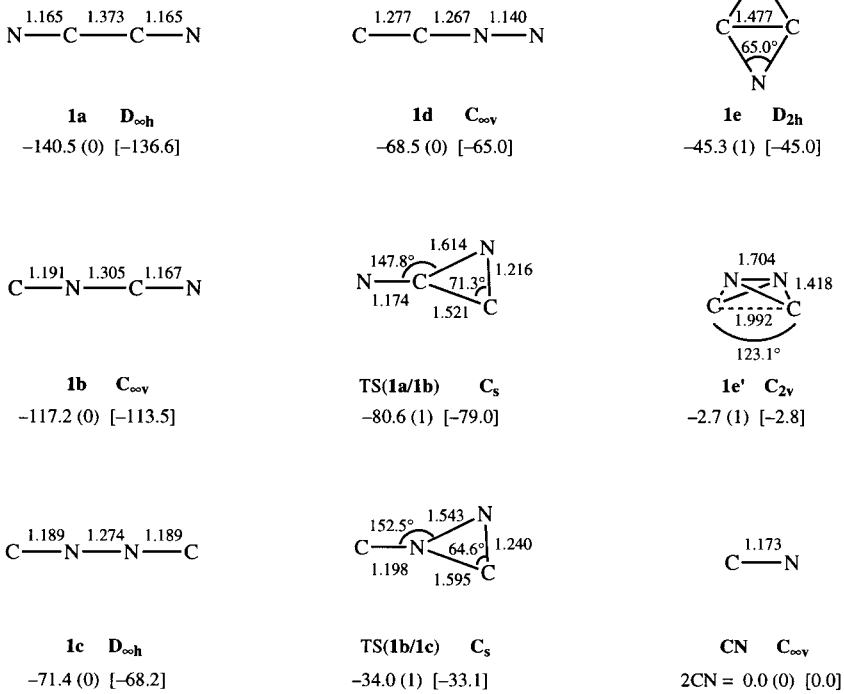

Figure 1. BP86/TZ2P results for C_2N_2 isomers (**1**): geometries (in Å, degrees), electronic energies (in kcal mol^{-1}) relative to 2 CN, number of imaginary frequencies (in parentheses), and 298 K enthalpies [in square brackets].

0947-6539/99/0501-0164 $ 17.50+.50/0 *Chem. Eur. J.* **1999**, *5*, No. 1

have a lower symmetry (C_s and C_1) and belong to the automerization of **1b** ($C^1N^2C^3N^4 \rightarrow N^2C^1N^4C^3$). They do find a cyclic transition state[4l] for the isomerization of **1c** to **1a**; however, this transition state is rather high in energy above **1c** (44.4 kcal mol^{-1} at B3LYP and 39.4 kcal mol^{-1} at CCSD(T)// B3LYP, respectively). Thus, caught in potential-energy wells of at least 34 kcal mol^{-1}, all three CN dimers are kinetically stable toward unimolecular isomerization at room temperature.

1.2. Flash vacuum thermolysis of norbornadienonazine: Our results are of relevance for the question why norbornadienonazine ($C_6H_6>C{=}N{-}N{=}C<C_6H_6$), even though it contains the CNNC entity and thus is a straightforward precursor of **1c**, on flash vacuum thermolysis (FVT) yields mainly CNCN (**1b**);[3] less than 1 % of **1c** was tentatively identified in the thermolysis product.[3d, 5]

While Sunil et al.[4e] had suggested a low-energy pathway from **1c** via **1a** to **1b**, the present study gave no indication for such a pathway. Another problem with a **1c**$\rightarrow$**1b** isomerization proceeding via **1a** is that it does not explain the predominant formation of the less stable **1b** on FVT at lower temperatures; the ratio of **1b**:**1a** on FVT of norbornadienonazine was approximately 2:1 at 450 °C and 1:2 at 800 °C.[3d] Moreover, **1b** was found to be remarkably stable towards rearrangement to **1a** under FVT conditions; the ratio of a 92:8 mixture of **1b**/**1a** remained unchanged on FVT at 500 °C, and only at 750 °C did it become 1:1.[3i] We therefore have to look for alternative interpretations of the formation of **1b**. In all likelihood, the precursor norbornadienonazine fragments on FVT in two steps:[3d] first, only one benzene moiety is split off under formation of an intermediate $C_6H_6>C{=}N{-}N{\equiv}C$, which may isomerize to the more stable $C_6H_6>C{=}N{-}C{\equiv}N$; thereafter, the second benzene moiety dissociates to furnish CNCN (**1b**). The isomerization of $C_6H_6>C{=}N{-}C{\equiv}N$ is, however, still a high-energy process. This is suggested by the results from a preliminary exploration of the potential-energy surface of the simple model system **5** [Eq. (4)].

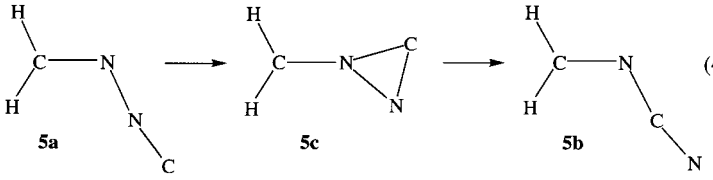

(4)

The interconversion of H_2CNNC (**5a**) to H_2CNCN (**5b**) proceeds via intermediate **5c**, which is 31.1 kcal mol^{-1} above **5a**; this is a lower limit for the reaction barrier. The 298 K reaction enthalpy for the conversion of **5a** to **5b** is -36.7 kcal mol^{-1}.

1.3. The C_2P_2 species: Our target molecule PCCP (**2a**) turns out to be a stable, linear CP dimer; the two monomeric units are bound by $\Delta H=-152.2$ kcal mol^{-1} at 298 K through a carbon–carbon bond of 1.336 Å (Figure 2). The weakly IR-active asymmetric C–P stretching vibration (P$\rightarrow\leftarrow$C$\leftarrow$C–P$\rightarrow$) has a frequency of 1245.8 cm^{-1}, that is, some 20 cm^{-1} higher than that of the CP radical (1226.3 cm^{-1}) and about 35 cm^{-1} lower than that of HCP (1281.2 cm^{-1}). The PC–CP bond is even somewhat stronger (16 kcal mol^{-1}) and shorter (0.04 Å) than the NC–CN bond. This is indicative of (partial) multiple C–C bond character. Thermodynamically, **2a** should therefore be just as stable a molecule as the well known cyanogen (**1a**). However, problems may be expected in view of a possibly low kinetic stability of **2a**, which stems from its rather small HOMO – LUMO gap of only 2.5 eV (see section 2.2); for comparison, the HOMO – LUMO gap in NCCN is 5.6 eV. Strategies to cope with the lower kinetic stability of **2a** are discussed in section 3.

However, there are more differences between **2** and **1** that become apparent when we couple the CP radicals through phosphorus. The weakening of the central bond R_2 (see Scheme 1), for example, is much more pronounced along the series **2a**–**2c** than for the linear nitrogen analogues **1a**–**1c**: the 298 K BDEs ($-\Delta H$) are 152.2, 68.7, and 7.5 kcal mol^{-1} (!) for PC–CP, CP–CP, and CP–PC, respectively (compare Figures 1 and 2). The fact that R_2 elongates from **2a** to **2b** to **2c** (from 1.336 to 1.709 to 2.216 Å) instead of decreasing as in **1a**–**1c** is, of course, simply due to the more diffuse character and larger effective size of the phosphorus atom compared with carbon or nitrogen. The external C–P bonds are somewhat elongated in **2a**–**2c** with respect to the isolated CP radical (1.577 Å).

More importantly, the linear CPCP (**2b**) and CPPC (**2c**) are no longer minimum-energy structures (Figure 2). Instead, structure **2b** represents a second-order saddle point connecting nonlinear, C_s symmetrical species **2b′**. The latter is the actual equilibrium structure of CP–CP with a C-P-C angle of 134.7°. Note, however, that the preference for the nonlinear **2b′** is only marginal: on the zero Kelvin potential-energy surface **2b′** is only 0.8 kcal mol^{-1} more stable than **2b**, whereas the 298 K CP–CP bond dissociation enthalpies for both are equal ($-\Delta H=68.7$ kcal mol^{-1}). It is therefore quite conceivable that another quantum chemical method may yield the linear **2b** as the equilibrium structure, but this would not affect our conception of the essential physics: CPCP (either **2b** or **2b′**) is much less prone to adapt a linear structure than PCCP; apparently, the CP–CP structure is highly flexible. In addition, the barrier for isomerization to PCCP (**2a**) is extremely low—effectively zero—and the nature of the corresponding reaction profile differs qualitatively from that for the nitrogen system (**1b**$\rightarrow$**1a**) in that it proceeds via an intermediate **2ab** (Figure 2). This unimolecular isomerization mechanism is shown in Equation (5).

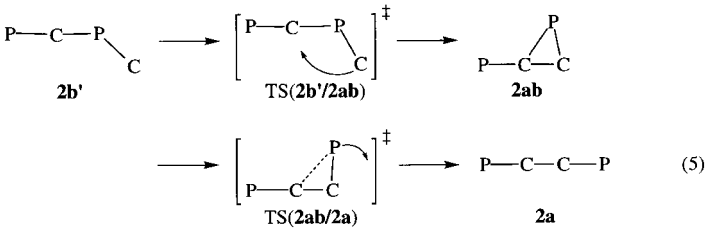

(5)

Intermediate **2ab** is 39 kcal mol^{-1} below CPCP (**2b′**) and 44.5 kcal mol^{-1} above PCCP(**2a**). The zero Kelvin activation energy $\Delta E^{\neq}$ for the first step in the isomerization is not more than +0.1 kcal mol^{-1} and the activation enthalpy $\Delta H^{\neq}$ (298 K)

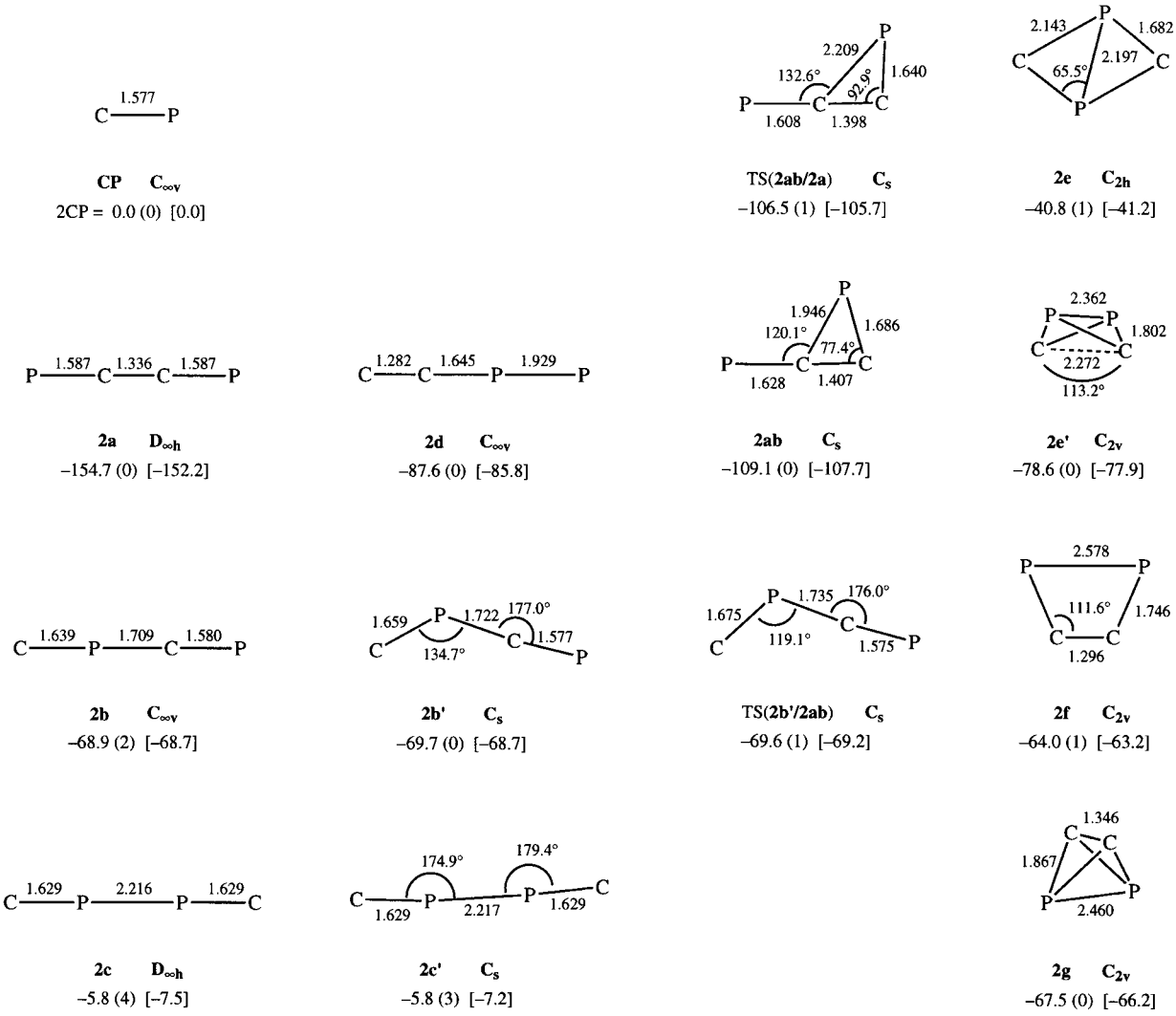

Figure 2. BP86/TZ2P results for C_2P_2 isomers (**2**) (see caption to Figure 1). Energies are relative to 2 CP.

is even slightly negative (-0.5 kcal mol^{-1}). Similarly, with 2 kcal mol^{-1}, the activation enthalpy for step 2 (**2ab** $\rightarrow$ **2a**) is very low. We conclude that, contrary to CNCN (**1b**), CPCP (**2b′**) is a labile species that easily converts to its more stable PCCP isomer **2a**.

The tendency to distort from linearity becomes even stronger when both CP radicals bind through phosphorus as in CPPC (**2c**), which is a fourth-order saddle point. Without aiming at completeness, we have performed a preliminary exploration of the C_2P_2 potential-energy surface in order to find minimum-energy structures that involve P–P bonding (see Figure 2). This revealed the C_{2v} symmetric **2e′**, which is at -77.9 kcal mol^{-1} (ΔH) relative to 2 CP. The P–P bond in **2e′** is 2.362 Å, that is, 0.146 Å longer than in the linear **2c**, and the P_2 unit is symmetrically bridged by each of the two carbon atoms with C–P bond lengths of 1.802 Å and a dihedral C-P-P-C angle of 113.2°. There is no C–C bond ($d_{CC} = 2.272$ Å). The puckered **2e′** may automerize through a 37 kcal mol^{-1} barrier (ΔH) associated with the planar C_{2h} symmetric transition state **2e**. The C atoms in the latter are arranged *trans* with respect to each other, each bridging the P_2 fragment asymmetrically. Species **2g**, another C_{2v} symmetric energy minimum, contains a firm C–C double bond of 1.346 Å; this molecule is 11.7 kcal mol^{-1} above **2e′**. Structures **2c′** and **2f** represent third- and first-order saddle points of higher energy, respectively; they will not be further discussed. Finally, an interesting linear C_2P_2 isomer not yet discussed is **2d**, the phosphorus analogue of **1d**, which one can view as a donor–acceptor bound codimer of C_2 and P_2 (vide supra). It is the second most stable, linear C_2P_2 isomer, 66.4 kcal mol^{-1} above PCCP (**2a**). The C–C, C–P, and P–P bond lengths in **2d** are 1.282, 1.645, and 1.929 Å, respectively.

1.4. Comparison with previous studies: The present results agree well with the available experimental and previous theoretical results. All reports about **2** refer to PCCP (**2a**). Our PC–CP bond dissociation enthalpy of 152.2 kcal mol^{-1} computed at BP86/TZ2P is nicely in between the experimental values of 148.9 ± 7.4[8a] and 157.4 ± 9.2 kcal mol^{-1}[8b] obtained through mass-spectrometric equilibrium measurements. Bock and Bankmann[8c] have calculated the geometry of PCCP using an MNDO approach. The MNDO value for the C–C bond length (1.36 Å; see Table 1) is 0.02 Å longer,

0947-6539/99/0501-0166 $ 17.50+.50/0 *Chem. Eur. J.* **1999**, *5*, No. 1

Table 1. Bond lengths of the central bond R_2 in the linear dimers **1a–c** of CN and **2a–c** of CP.[a]

	NC–CN (**1a**)	CN–CN (**1b**)	CN–NC (**1c**)	PC–CP (**2a**)	CP–CP (**2b**)	CP–PC (**2c**)
theoretical						
this work[b]	1.373	1.305	1.274	1.336	1.709	2.216
MNDO[8c]				1.36		
MP2[4c]	1.381	1.318	1.279			
CEPA[4f]	1.395	1.322	1.294			
B3LYP[4l]	1.375	1.307	1.274			
experimental						
HR-IR[15a]	1.389					
HR-Raman[15b]	1.380					
MW[3c]		1.314				
ED	1.388[15c]	1.312[3p]				
X-ray[3q]		1.300				

[a] See Scheme 1. [b] Computed at the BP86/TZ2P level.

whereas that for the C–P bond (1.44 Å) is 0.14 Å shorter than our DFT results.

Our values for the internal bond lengths R_2 of **1a** and **1b** are generally in good agreement with those obtained by other theoretical calculations and by a variety of experimental methods (Figure 1, Table 1). Experimentally, the NC–CN bond strength was determined to be 134.7 ± 4.2 kcal mol^{-1}[15d], only 1.9 kcal mol^{-1} less than our value. To our knowledge, no experimental geometry or BDE values have been reported for **1c**. Sunil et al.[4e] have computed an NC–CN bond dissociation energy of 149.9 kcal mol^{-1} at MP4SDTQ (using spin-projected calculations for CN to correct for spin contamination) that deviates by $+9$ kcal mol^{-1} from our BP86/TZ2P value ($-\Delta E$) and by $+15$ kcal mol^{-1} from the experimental result ($-\Delta H$).[15d]

2. C_2P_2 and C_2N_2: electronic structure and bonding: In this section, we try to understand the nature of the bonding in the target molecule PCCP (**2a**). To this end, the electronic structure of the linear $(CP)_2$ systems (**2a–2c**) is analyzed and compared with that of the linear $(CN)_2$ species (**1a–c**). Thereafter, we address the question why PCCP and the CN dimers are linear, whereas CPCP and especially CPPC tend to possess a nonlinear geometry.

2.1. CP and CN: electronic structure and orbital interactions: The valence levels of the CN and CP fragments are displayed in Figure 3, together with a schematic representation of the corresponding orbitals. At the lower end of the orbital spectrum, we have the σ_{HOMO-1} (i.e., 3σ for CN and 5σ for CP), which is given by the bonding 2s(C)+2s(N) or 2s(C)+3s(P) combination. This low-energy orbital as well as the high-energy unoccupied 6σ(CN) and 8σ(CP) are of minor importance for the central bond in the CN and CP dimers **1a–c** and **2a–c**. Instead, it is the frontier orbitals in the middle of the orbital spectrum that determine the bonding capabilities of the CN and CP monomers: in σ symmetry they are the σ_{HOMO} and the σ_{SOMO} (i.e., 4σ and 5σ for CN; 6σ and 7σ for CP), and in π symmetry they are the π_{HOMO} and the π_{LUMO} (i.e., 1π and 2π for CN; 2π and 3π for CP). Both σ_{HOMO} and σ_{SOMO} are essentially nonbonding orbitals. The former provides the axial N or P lone pair, whereas the latter carries the

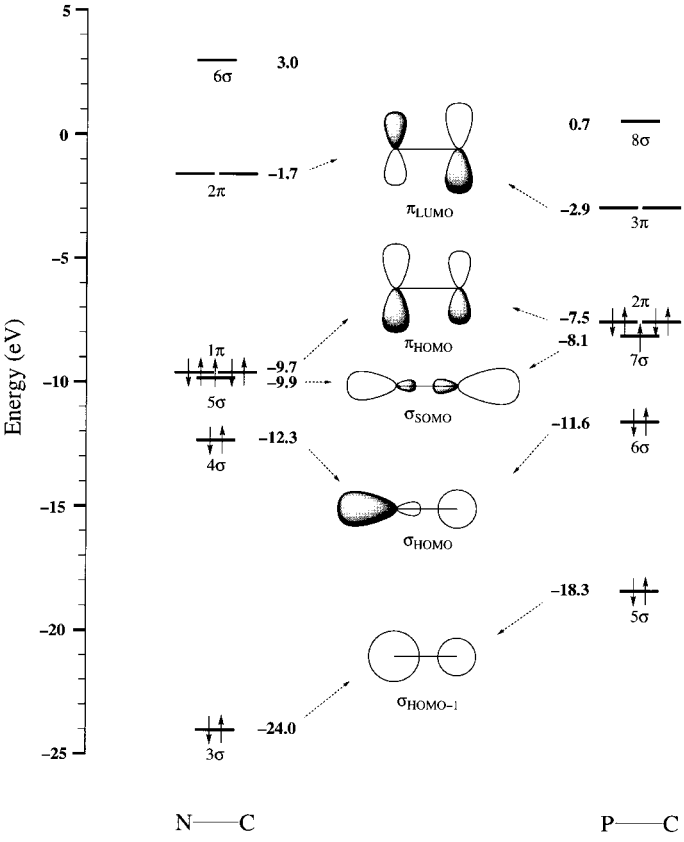

Figure 3. Valence orbital levels of CN and CP.

unpaired electron. The doubly degenerate π_{HOMO} constitutes the two π bonds in CN and CP; its antibonding counterpart is the unoccupied π_{LUMO}.

How do these fragment orbitals interact in the dimers? In σ-symmetry, the SOMOs on the two monomers provide the electron-pair bond by forming the $(\sigma_{SOMO}+\sigma_{SOMO})^2$ configuration (**A**). Not being separated by a large HOMO–LUMO gap from the occupied orbitals, the SOMO is furthermore

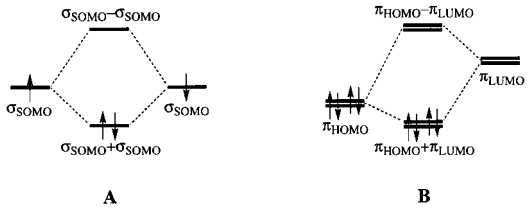

predestined to enter into a subtle interplay of stabilizing and destabilizing interactions with the closed-shell σ_{HOMO} of the other fragment: i) the SOMO may act as an unoccupied orbital *accepting* charge from the σ_{HOMO}, which leads to stabilization; or ii) it may act as an occupied orbital whose electron experiences Pauli repulsion with the same-spin electron in the σ_{HOMO}. Another important Pauli-repulsive component in σ symmetry stems from the destabilizing four-electron-two-orbital $\sigma_{HOMO} \pm \sigma_{HOMO}$ interaction (see also Figure 5).

In π symmetry, there is a stabilizing donor–acceptor interaction between the doubly degenerate π_{HOMO} and π_{LUMO} (**B**) causing two partial π bonds. They are opposed by the

Pauli-repulsive four-electron-two-orbital $\pi_{HOMO} \pm \pi_{HOMO}$ interaction. Note the difference in nature between the σ bond (electron-pair bonding) and the π bonds (donor–acceptor bonding).

Before we discuss the actual energetic effects of the various interfering mechanisms, let us take a more detailed look at the shape of the frontier orbitals (see contour plots in Figure 4).

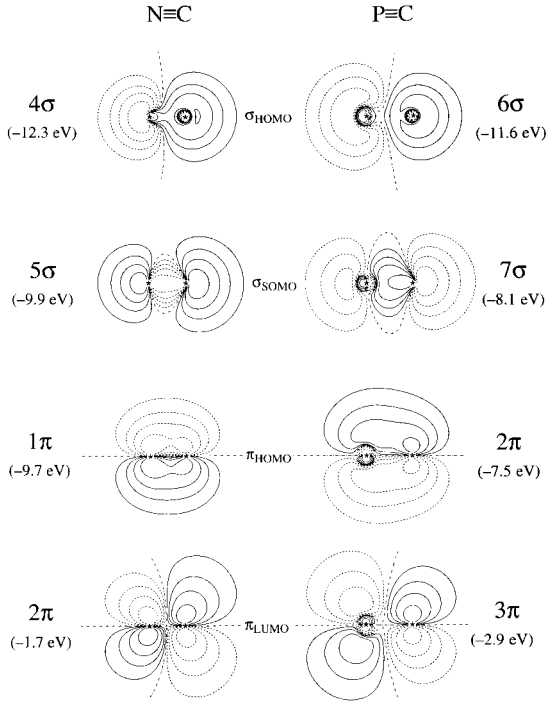

Figure 4. Contour plots and energies (eV) of CN and CP frontier orbitals (scan values: 0.0, ±0.02, ±0.05, ±0.1, ±0.2, ±0.5).

Note that the difference in appearance between the CN and CP orbitals is rather small, in spite of the fact that phosphorus is clearly less electronegative than nitrogen. This has the following reason. The σ_{SOMO}, for example, arises from the bonding $2p_\sigma(C)+p_\sigma(X)$ combination with an antibonding admixture of 2s(C), leading to an essentially nonbonding character and the large characteristic lobe on carbon (X = N, P). The $p_\sigma(X)$ in CN, that is, the nitrogen $2p_\sigma$, is energetically in between the carbon 2s and 2p AOs. However, the energy of the $p_\sigma(X)$ in CP, that is, the phosphorus $3p_\sigma$, is much higher and approaches that of the $2p_\sigma(C)$. As a result, the 2s(C) component becomes smaller, but this is out weighed by an increasing $2p_\sigma(C)$ contribution. Overall, the σ_{SOMO} becomes somewhat more localized on C as we go from CN (49%) to CP (61%). Likewise, the σ_{HOMO} gets a somewhat higher 2s(C) component going from CN to CP, but the appearance is very similar in both radicals. The π_{HOMO} and π_{LUMO} result from the bonding and antibonding $2p_\pi(C) \pm p_\pi(X)$ combinations, respectively. In CN, the π_{HOMO} has a higher amplitude on the more electronegative N and the π_{LUMO} on the more electropositive C. The contributions from carbon and phosphorus in CP are more in balance. Yet both the π_{HOMO} and π_{LUMO} do have more extended lobes on phosphorus simply because this atom is more diffuse and larger than carbon.

An important feature of the CX orbitals (X = N, P) is their delocalized nature. In particular the SOMO, carrying the unpaired electron, has significant amplitude at both ends of the diatomic. This causes CN and CP to be ambident radicals. Thus, in terms of simple valence bond (VB) structures, they are best represented as resonances **C** and **D**.

C **D**

As a direct consequence, CN and CP may form electron-pair bonds either through C–C, C–X or X–X coupling (X = N, P) leading to **1a–c** and **2a–c**. However, it is also clear that the SOMO is not evenly distributed, having a more extended and higher amplitude lobe at the carbon side. On this ground, the strength of the electron-pair bond **A** and thus the stability of the dimer should decrease in the order XC–CX > CX–CX > CX–XC. This trend may be reinforced by the fact that the $\sigma_{HOMO} \pm \sigma_{HOMO}$ repulsion increases in the same order because the σ_{HOMO}—the N or P lone pair—is either more extended (CP 6σ) or of higher amplitude (CN 4σ) on the hetero atom.

2.2. Bonding in linear CP and CN dimers: quantitative trends: The qualitative considerations above nicely match the trends in relative stability along the series **1a–c** and **2a–c** discussed in section 1. However, underneath the surface of the overall bond dissociation enthalpy, the situation is more complex as we show in the following quantitative analysis (see Table 2 and Figure 5). The first step of forming the dimer is the adaption of the monomer's geometry to the situation in the

Table 2. Analysis of the central bond R_2 in **1a–c** and **2a–c**.[a,b]

	NC–CN (**1a**)	CN–CN (**1b**)	CN–NC (**1c**)	PC–CP (**2a**)	CP–CP (**2b**)	CP–PC (**2c**)
bond energy decomposition [kcal mol^{-1}]						
ΔE_σ	–230.0	–306.9	–360.7	–243.3	–168.3	–71.5
ΔE_π	–58.2	–79.4	–85.8	–77.6	–56.7	–32.6
ΔE_{oi}[c]	–288.2	–386.3	–446.5	–320.9	–225.0	–104.1
ΔE^0	144.3	265.5	371.3	161.5	149.6	91.0
ΔE_{int}[d]	–143.9	–120.8	–75.2	–159.4	–75.4	–13.1
ΔE_{prep}	3.4	3.6	3.8	4.7	6.5	7.3
ΔE[e]	–140.5	–117.2	–71.4	–154.7	–68.9	–5.8
fragment orbital overlaps $\langle CX \mid CX\rangle$[f,g]						
$\langle \sigma_{SOMO} \mid \sigma_{SOMO}\rangle$	0.46	0.31	0.21	0.43	0.27	0.16
$\langle \sigma_{HOMO} \mid \sigma_{HOMO}\rangle$	0.26	0.31	0.37	0.22	0.27	0.29
$\langle \sigma_{HOMO} \mid \sigma_{SOMO}\rangle$	0.35	0.41/0.24	0.28	0.32	0.41/0.19	0.22
$\langle \pi_{LUMO} \mid \pi_{LUMO}\rangle$	0.33	0.20	0.15	0.18	0.21	0.25
$\langle \pi_{HOMO} \mid \pi_{HOMO}\rangle$	0.09	0.12	0.14	0.13	0.10	0.07
$\langle \pi_{HOMO} \mid \pi_{LUMO}\rangle$	0.21	0.25/0.14	0.16	0.17	0.14/0.20	0.15
CX fragment orbital populations[f,h]						
σ_{SOMO}	1.18	1.51/1.10	1.44	1.11	1.35/0.90	1.13
σ_{HOMO}	1.79	1.52/1.79	1.51	1.86	1.74/1.84	1.76
π_{LUMO}	0.08	0.09/0.11	0.10	0.16	0.14/0.12	0.09
π_{HOMO}	1.93	1.88/1.94	1.91	1.83	1.87/1.83	1.90

[a] Carried out at the BP86/TZ2P level. [b] See Scheme 1. [c] $\Delta E_{oi} = \Delta E_\sigma + \Delta E_\pi$. [d] $\Delta E_{int} = \Delta E_{oi} + \Delta E^0$. [e] $\Delta E = \Delta E_{int} + \Delta E_{prep}$. [f] σ_{HOMO}, σ_{SOMO}, π_{HOMO}, π_{LUMO} are 4σ, 5σ, 1π, 2π for CN, and 8σ, 9σ, 3π, 4π for CP (Figures 3 and 4). [g] In the case of CX–CX (X = P, N): $\langle \phi$ left CX $\mid \phi$ right CX$\rangle / \langle \phi$ right CX $\mid \phi$ left CX$\rangle$. [h] In the case of CX–CX (X = P, N): population of ϕ in left CX/population of ϕ in right CX.

0947-6539/99/0501-0168 $ 17.50+.50/0 *Chem. Eur. J.* **1999**, *5*, No. 1

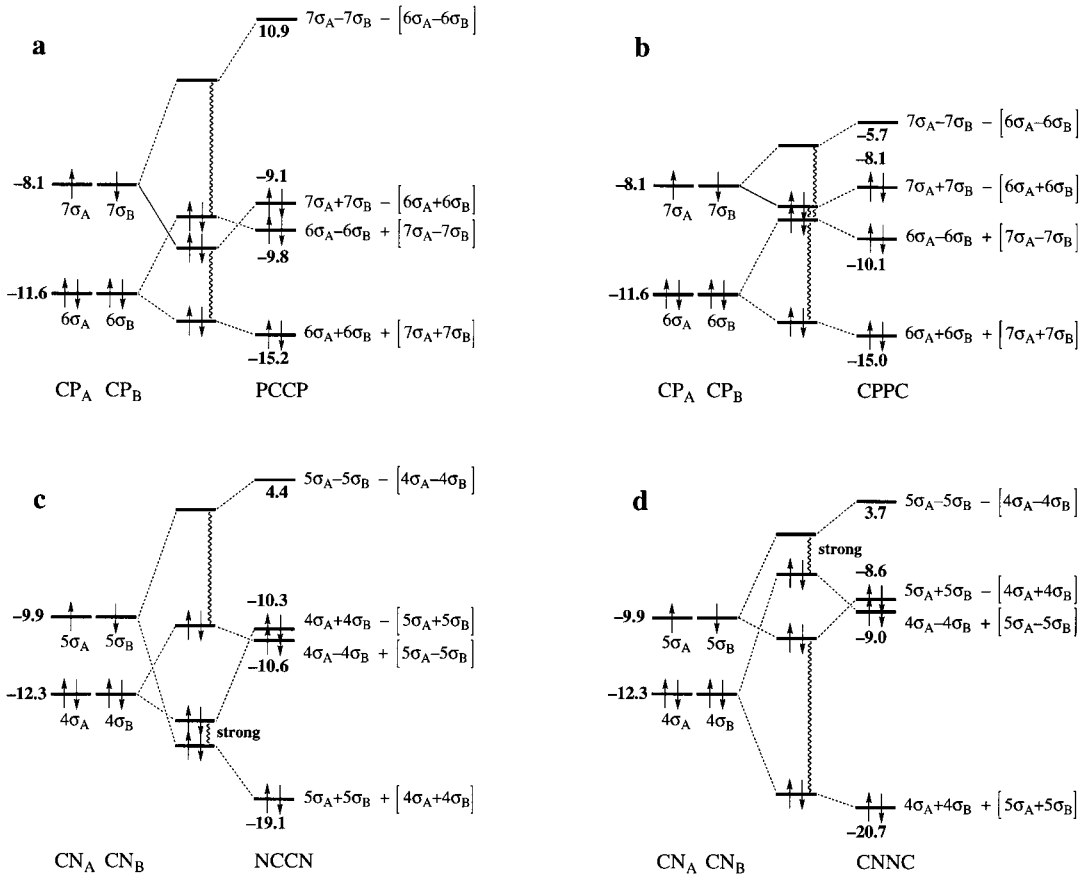

Figure 5. Schematic σ orbital interaction diagram for: a) PC–CP, b) CP–PC, c) NC–CN, and d) CN–NC (MO and FMO energies in eV). Left panel: FMOs. Central panel: zeroth-order interaction, that is, no $\sigma_{SOMO}/\sigma_{HOMO}$ mixing. Right panel: final situation including all interactions.

composite molecule, that is, a slight reduction or increase of the C–X bond length (X = N, P). The associated preparation energy ΔE_{prep} is rather small in all cases, that is, 4–7 kcal mol^{-1} (Table 2). It has no influence on the overall trend and will not be further discussed. The actual interaction energy ΔE_{int} between the prepared monomers decreases in both the CN dimers (from −143.9 to −75.2 kcal mol^{-1}, see Table 2) and in the linear CP dimers (from −159.4 down to only −13.1 kcal mol^{-1}) as we go from C–C to C–X to X–X coupling. However, these qualitatively similar trends in the two isomeric series turn out to have quite different origins. In the CN dimers, the reduction in bond strength is caused by an enormous increase in ΔE^0 repulsion (from 144.3 to 371.3 kcal mol^{-1}) if we go from **1a** to **1c**. The increase in ΔE^0 is counteracted, but not compensated, by a sizeable increase in ΔE_{oi} (from −288.2 to −446.5 kcal mol^{-1}). In contrast, in the CP dimers the bond strength decreases because of a weakening of the bonding orbital interactions ΔE_{oi} (from −320.9 to −104.1 kcal mol^{-1}), which is particularly pronounced for the σ bond ΔE_σ, in spite of an opposite trend of the repulsion energy ΔE^0, which actually decreases (from 161.5 to 91.0 kcal mol^{-1}).

The increase in Pauli repulsion along the CN dimers **1a–c** is caused by the increase in overlap between the closed-shell σ_{HOMO} and π_{HOMO} orbitals (Table 2), respectively, which have higher amplitudes on nitrogen (Figure 4). In NCCN (**1a**), the repulsive overlap between the CN σ_{HOMO}'s, for example, is relatively small (0.26) leading to a correspondingly weak interaction. This is illustrated by the relatively small separation between the zeroth-order bonding $\sigma_{HOMO}+\sigma_{HOMO}$ and antibonding $\sigma_{HOMO}-\sigma_{HOMO}$ combination belonging to the fictitious situation in which only $\sigma_{HOMO}/\sigma_{HOMO}$ and $\sigma_{SOMO}/\sigma_{SOMO}$ interaction has occurred, but *not yet* mixing between σ_{SOMO} and σ_{HOMO} (see orbital interaction diagram in Figure 5c, central panel). In CNNC (**1c**), the overlap between the σ_{HOMO}'s rises to 0.37 and, likewise, the gap between zeroth-order bonding and antibonding combinations increases (Figure 5d). But what about the increase in stabilizing orbital interactions along **1a–c**? This does not correlate with the bond overlap $\langle\sigma_{SOMO}|\sigma_{SOMO}\rangle$, which, as qualitatively predicted, decreases from 0.46 down to 0.21. Here, the $\sigma_{SOMO}/\sigma_{HOMO}$ interaction comes into play. Indeed, for the zeroth order the $\sigma_{SOMO}/\sigma_{SOMO}$ interaction decreases along **1a–c**, as indicated by the reduced splitting between the occupied $\sigma_{HOMO}+\sigma_{HOMO}$ and the unoccupied $\sigma_{HOMO}-\sigma_{HOMO}$ in the zeroth-order panels for **1a** and **1c** (Figures 5c and 5d). Thus, for the zeroth order, the $\sigma_{SOMO}+\sigma_{SOMO}$ descends strongly and comes out close to, in fact even below, the $\sigma_{HOMO}+\sigma_{HOMO}$. This causes strong mutual repulsion that pushes the $\sigma_{HOMO}+\sigma_{HOMO}$ upward (Figure 5c, right panel). As a result, ΔE_σ and ΔE_{oi} become less bonding in **1a**. In contrast, in **1c** it is the occupied $\sigma_{HOMO}-\sigma_{HOMO}$ that approaches, in the zeroth order, the unoccupied $\sigma_{SOMO}-\sigma_{SOMO}$ from below (Figure 5d, central panel). The resulting strong-stabilizing donor–acceptor interaction has the effect

of making ΔE_σ and ΔE_{oi} more bonding. This effect, which leads to the increase in ΔE_σ and ΔE_{oi} along **1a–c**, may also be regarded as an attempt of the system to alleviate the strong $\sigma_{HOMO} \pm \sigma_{HOMO}$ repulsion. A similar mechanism is active in π symmetry. Furthermore, note that in **1a** the $\sigma_{HOMO}+\sigma_{HOMO}$ ends up at low energy (−19.1 eV), whereas it becomes the HOMO in CNNC (−8.6 eV). For a more detailed discussion on the nature of the central bond in CN dimers and, in particular, on the interference between electron-pair bonding and closed-shell/closed-shell Pauli repulsion, we refer to ref. [4i].

What causes the Pauli repulsive and bonding orbital interaction to behave differently, that is, why do both ΔE^0 and ΔE_{oi} decrease from **2a** to **2c**? In the first place, the CP orbitals are more extended and diffuse at the P side. This leads to smaller overlap, which reaches a lower maximum at longer bond length R_2, as soon as phosphorus becomes involved in the central bond (see Table 1). Thus, the Pauli repulsion contained in ΔE^0 and, even more so, the bonding orbital interactions ΔE_{oi} decrease along **2a–c** instead of increasing as they do along **1a–c**. Secondly, the decrease in $\sigma_{SOMO}+\sigma_{SOMO}$ electron-pair bonding, if we go from **2a** to **2c**, is no longer compensated by a strongly stabilizing $\sigma_{HOMO}/\sigma_{SOMO}$ interaction; the $\sigma_{HOMO} - \sigma_{HOMO}$ just does not come close enough to the empty $\sigma_{SOMO} - \sigma_{SOMO}$ (compare Figures 5a–d). This is simply due to the smaller $\sigma_{HOMO} \pm \sigma_{HOMO}$ splitting in the CP dimer together with the larger $\sigma_{HOMO}/\sigma_{SOMO}$ gap in CP (3.5 eV) compared with CN (2.4 eV; see Figures 3 and 5).

The carbon–carbon bonds in **2a** and **1a**, the most stable CP and CN dimer, respectively, are of comparable strength($\Delta E =$ −154.7 and −140.5 kcal mol^{-1}, respectively) and the differences in the bonding mechanisms are subtle (Table 2). As mentioned above, the $\sigma_{SOMO}/\sigma_{HOMO}$ repulsion is less pronounced in PCCP. This leads to a somewhat stronger orbital (ΔE_{oi}) and overall interaction (ΔE), a slight reduction of the bond length R_2 (1.336 Å in **2a** versus 1.373 Å in **1a**), and a small increase of $\pi_{HOMO} \pm \pi_{HOMO}$ repulsion contained in ΔE^0 (Table 2). Furthermore, the $\sigma_{SOMO}+\sigma_{SOMO}$ of **2a** does not drop below the $\sigma_{HOMO}+\sigma_{HOMO}$ and turns into the highest occupied σ orbital at −9.1 eV, unlike the situation in NCCN in which it ends up at −19.1 eV (compare Figures 5a and 5c). Note also that in PC–CP, the π-bonding contribution ΔE_π (−77.6 kcal mol^{-1}), although much smaller than ΔE_σ (−243.3 kcal mol^{-1}), is still substantial in the sense that it furnishes half of the overall bond energy ΔE. Thus, in terms of simple valence bond structures, the nature of **2a** is best represented by resonance **E**.

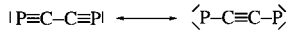

E

The most important difference between **2a** and **1a** is the much smaller HOMO–LUMO gap in the former: 2.5 eV versus 5.6 eV. This difference is already predetermined by the π electronic structures of the diatomic fragments. The HOMO and LUMO are the zeroth-order antibonding $\pi_{HOMO} - \pi_{HOMO}$ and bonding $\pi_{LUMO}+\pi_{LUMO}$ combinations of fragment orbitals, respectively, in both **2a** and **1a**. Because the $2p_\pi$(C) and $3p_\pi$(P) atomic orbitals in CP do not overlap as efficiently as the $2p_\pi$(C) and $2p_\pi$(N) in CN do, the π_{HOMO}/π_{LUMO} gap of CP and the HOMO–LUMO gap of PCCP are smaller than the corresponding ones in CN and NCCN; the HOMO–LUMO gap of PCCP is even smaller than that of the reactive CNNC (5.4 eV). We conclude that in all likelihood, our target molecule **2a** is also kinetically labile, in spite of its high thermodynamic stability. For example, its tendency to polymerize may be even higher than that of CNNC. This conclusion is in line with the recent experimental observation that promising direct precursors of **2a** appear to fragment and decompose under the conditions of their formation.[9] A potential remedy is discussed in section 3.

2.3. Linear versus nonlinear geometry: So far, we have compared linear CP and CN dimers, but actually **2b** and **2c** are higher order saddle points. In contrast to their nitrogen analogues, **2b** and **2c** tend to adapt nonlinear structures (**2b′** and **2e′**, respectively; see Figure 2 and Results and Discussion, section 1). Why is that so? To answer this question we have analysed how the CX/CX bonding changes on bending **2a–c** and, for comparison, **1a–c** as shown in Equation (6).

(6)

The results, that is, the changes in ΔE_{oi} and ΔE^0, and overlaps on bending the system, are summarized for **2a**, **2c**, **1a**, and **1c** in Table 3.

Table 3. Changes in bonding on bending the CP/CP or CN/CN bond as shown in Equation (6).[a]

	NC–CN (**1a**)	CN–NC (**1c**)	PC–CP (**2a**)	CP–PC (**2c**)
change in bond energy terms [kcal mol^{-1}]				
$\Delta\Delta E_{oi}$	−12.2	1.2	−27.3	−3.0
$\Delta\Delta E^0$	26.2	6.6	41.1	2.4
$\Delta\Delta E_{int}$[b]	14.0	7.8	13.8	−0.6
change in fragment orbital overlap $\langle AB \mid CD \rangle$[c]				
$\Delta\langle\pi_{HOMO} \mid \sigma_{SOMO}\rangle$	0.15	0.12	0.18	0.09
energy gap between fragment orbitals [eV][c]				
π_{HOMO}/σ_{SOMO}	0.2	0.2	0.6	0.6

[a] BP86/TZ2P level. [b] $\Delta\Delta E_{int} = \Delta\Delta E_{oi} + \Delta\Delta E^0$. [c] σ_{SOMO}, π_{HOMO} are 5σ, 1π for CN, and 7σ, 2π for CP, respectively (Figures 3 and 4).

The question of bending or not bending is a subtle one, but it is mainly determined by the trend in Pauli-repulsion that is part of ΔE^0 (Table 3). In all cases, bending is opposed by an increase in repulsion ($\Delta\Delta E^0 > 0$), especially on C–C coupling, but much less so for X–X coupling, whereas $\Delta\Delta E_{oi}$ either favors (**2a**, **2c**, **1a**) or only weakly resists the distortion (**1c**). The increase in repulsion on bending, $\Delta\Delta E^0$, is strongest for **2a** (41.1 kcal mol^{-1}), but weakest for **2c** (2.4 kcal mol^{-1}), which causes the latter isomer to eventually distort toward **2e′**. The CPCP isomer, for which the results are not shown in Table 3, is an intermediate case with a very shallow potential-energy surface between linear **2b** and nonlinear **2b′** and an extremely weak preference for the latter structure at our BP86/TZ2P level of theory. As pointed out in section 1.3, other theoretical methods or levels might reverse the ener-

0947-6539/99/0501-0170 $ 17.50+.50/0 *Chem. Eur. J.* **1999**, *5*, No. 1

getic order of linear (**2b**) and nonlinear (**2b′**) CPCP structure, but without changing the physical picture of an increasing bias toward nonlinearity along the series PCCP, CPCP, and CPPC.

The trend in the $\Delta\Delta E_{oi}$ term is, amongst others, the result of decreasing $\sigma_{SOMO}/\sigma_{HOMO}$ overlaps when the system is twisted (not shown in Table 3). This causes the four-electron interaction between the zeroth-order $\sigma_{SOMO}+\sigma_{SOMO}$ and $\sigma_{HOMO}+\sigma_{HOMO}$, contained in the ΔE_{oi} term, to become less repulsive, especially for NCCN and much less so for CNNC (see Figure 5). The trend in $\Delta\Delta E^0$ correlates with the overlap of the π_{HOMOx} on one fragment with the σ_{SOMO} on the other fragment. This is zero by symmetry in the linear species (see Scheme 2, left). However, on bending, as the lobe of the σ_{SOMO} moves out of the nodal plane of the π_{HOMOx}, overlap begins to build up and reaches values of 0.18, 0.09, 0.15, and 0.12 for **2a**, **2c**, **1a**, and **1c**, respectively (see Scheme 2, right, and Table 3). The increase in overlap on bending is largest for PC–CP and smallest for CP–PC, because both the σ_{SOMO} and π_{HOMO} of CP have a somewhat higher weight on carbon than the σ_{SOMO} and π_{HOMO} of CN as explained in section 2.1.

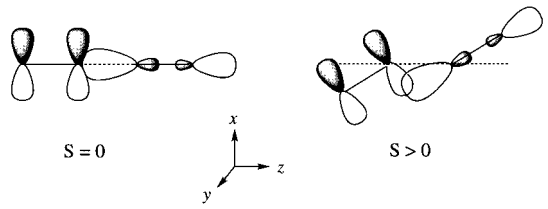

Scheme 2.

The overlap $\langle\pi_{HOMO}|\sigma_{SOMO}\rangle$ and repulsion ΔE^0 can be further decreased by reducing the dihedral angle A-B-C-D of the bent dimer, shown on the right side in Equation (6) and Scheme 2, in which it is 180°. For **2c**, this leads ultimately to equilibrium structure **2e′**, in which the dihedral angle amounts to 113.2° (Figure 2). The corresponding nitrogen structure **1e′** is a transition state for automerization of linear CNNC (Figure 1).

3. Stabilization of PCCP through coordination: Our target molecule PCCP (**2a**) turns out to be thermodynamically stable, but it is likely to be kinetically labile (vide supra). A counter measure against this lability may be coordination to a transition metal, as illustrated by the stabilization of **1b** in $[Cr(CO)_5CNCN]$.[12] This might lead to an isolable complex, in which **2a** is electronically stabilized and/or sterically protected. We have therefore analyzed the model complexes $[Cr(CO)_5PCCP]$ (**3**) and $[(CO)_5Cr(PCCP)Cr(CO)_5]$ (**4**). The results are shown in Figure 6.

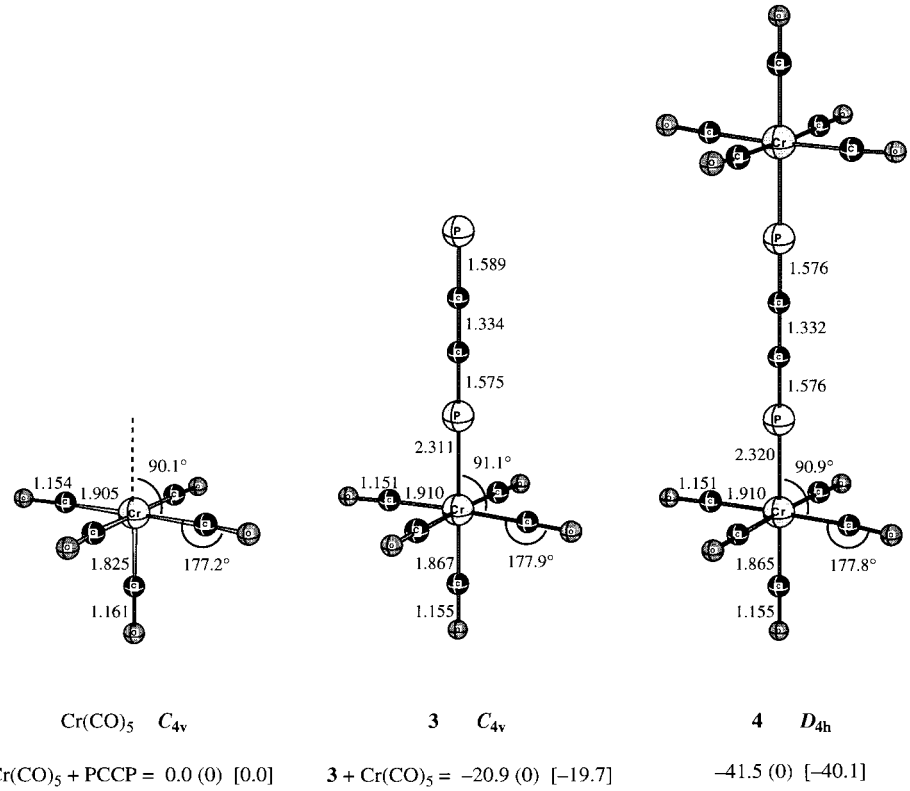

Figure 6. BP86/TZ2P results for $\{Cr(CO)_5\}$, **3**, and **4** (see caption to Figure 1). Energies are relative to PCCP and $2\{Cr(CO)_5\}$.

Indeed, the D_{4h} symmetric complex **4** turns out to be stable towards dissociation at room temperature, although the coordination bond is of moderate strength only. The 298 K enthalpy for dissociation of **4** into $\{Cr(CO)_5\}$ and **3** is 20.4 kcal mol^{-1} and that for dissociation of **3** into $\{Cr(CO)_5\}$ and PCCP is 19.7 kcal mol^{-1}, while the Cr–P bond lengths in **3** and **4** amount to 2.3 Å. The C–P bonds of the PCCP unit in **4** are slightly shortened, by 0.011 Å, with respect to those in uncoordinated **2a** (compare Figures 2 and 6). In line with this, the frequency of the weakly IR-active asymmetric C – P stretch vibration increases by 47 cm^{-1} from **2a** (1245.8 cm^{-1}) to **4** (1293.2 cm^{-1}).[17] The energy needed to rotate a $\{Cr(CO)_5\}$ group in **4** by 45° around the Cr – Cr main axis is less than 0.1 kcal mol^{-1}, and we conclude that the $\{Cr(CO)_5\}$ groups rotate freely with respect to each other. To assess the influence of the nonlocal DFT method applied, we have also computed the (first) [Cr]–P bond dissociation energies (zero K, no ZPE correction) of **4** and **3** using our standard BP86 as well as the PW91[18] and BLYP[13h, 13i, 19] approaches; in all cases the TZ2P basis was employed. The BP86 bond energies (20.9 and 20.6 kcal mol^{-1}) turn out to be close to and, in fact, in between the slightly stronger PW91 (23.8 and 23.4 kcal mol^{-1}) and the slightly weaker BLYP bond energies (18.6 and 18.3 kcal mol^{-1}; not shown in Table 4).

  0947-6539/99/0501-0171 $ 17.50+.50/0

Table 4. Analysis of the $(CO)_5Cr{-}L$ coordinative bond.

	$-\{(PCCP)Cr(CO)_5\}$[a,b] (in **4**)	$-PCCP$[a] (in **3**)	$-CNCN$[c]	$-CO$[c]
bond energy decomposition [kcal mol^{-1}]				
ΔE_σ	−26.5	−26.7	−39.9	−37.4
ΔE_π	−23.8	−24.9	−45.4	−37.8
ΔE_{oi}[d]	−50.3	−51.6	−85.3	−75.2
ΔE^0	27.4	29.9	32.8	31.0
ΔE_{int}[e]	−22.9	−21.7	−52.5	−44.2
ΔE_{prep}	2.3	0.8	2.9	2.0
ΔE[f]	−20.6	−20.9	−49.6	−42.2
fragment orbital overlaps $\langle\{Cr(CO)_5\}\,\vert\,L\rangle$				
$\langle 10a_1 \vert \sigma_{HOMO}\rangle$	0.37[g]	0.27[h]	0.44	0.44
$\langle 8e_1 \vert \pi^*_{LUMO}\rangle$	0.10	0.11	0.14	0.17
fragment orbital populations [e]				
$\{Cr(CO)_5\}$:$10a_1$	0.32	0.35	0.32	0.32
L:σ_{HOMO}	1.61[i]	1.71[j]	1.63	1.62
$\{Cr(CO)_5\}$:$8e_1$	1.85	1.84	1.78	1.83
L:π^*_{LUMO}	0.12	0.13	0.22	0.20

[a] This work: BP86/TZ2P level. [b] All values equal for D_{4h} and C_{4v} symmetric **4**. [c] BP86 from ref. [12c]. [d] $\Delta E_{oi} = \Delta E_\sigma + \Delta E_\pi$. [e] $\Delta E_{int} = \Delta E_{oi} + \Delta E^0$. [f] $\Delta E = \Delta E_{int} + \Delta E_{prep}$. [g] $\langle 10a_1 \vert \sigma_{HOMO-1}\rangle = 0.11$. [h] $\langle 10a_1 \vert \sigma_{HOMO-1}\rangle = 0.28$. [i] Population of $\{Cr(CO)_5PCCP\}$ σ_{HOMO-1} is 2.00 e. [j] Population of PCCP σ_{HOMO-1} is 1.83 e.

We have also analyzed the Cr–P bond in **3** and **4**. In Table 4, our results are collected and compared with those from literature for the $Cr(CO)_5{-}CNCN$ and $Cr(CO)_5{-}CO$ bonds. The Cr–PCCP bond is furnished by relatively well-balanced σ donation [from the σ_{HOMO} and, to a lesser extent, σ_{HOMO-1} of PCCP to the $3d_\sigma$-derived LUMO of $\{Cr(CO)_5\}$] and π backdonation [from the $3d_\pi$-derived HOMO of $\{Cr(CO)_5\}$ to the π_{LUMO} of PCCP]. In **3**, the σ and π components of the bonding orbital interactions between $\{(CO)_5Cr\}$ and PCCP amount to −26.7 and −24.9 kcal mol^{-1}, leading, together with the repulsive ΔE^0 term (29.9 kcal mol^{-1}) and a small ΔE_{prep} (0.6 kcal mol^{-1}), to the overall bond energy $\Delta E = -20.9$ kcal mol^{-1}. The σ donor and π acceptor orbitals of PCCP are slightly stabilized and destabilized, respectively, but in spite of this the HOMO–LUMO gap is further reduced, that is, from 2.5 eV in **2a** to 2.3 eV in **3**, instead of being increased. How is this possible? The answer is very simple: it is not the σ_{HOMO} (which is stabilized on complexation), but the relatively high energy π_{HOMO} that provides the overall HOMO of PCCP, and this π_{HOMO} is somewhat more destabilized by the $3d_\pi$-type HOMO of $\{Cr(CO)_5\}$ than the π_{LUMO}. Thus, one may expect that a kinetic stabilization of the PCCP unit in **3** is not primarily achieved by an increase of the HOMO–LUMO gap, but instead through steric protection. The reactivity will in principle also be reduced due to the fact that the frontier orbitals of **3** are delocalized more or less over the entire complex and have, naturally, somewhat less amplitude on PCCP than the HOMO and LUMO of the isolated ligand they mainly stem from. The situation is very similar for the Cr–P bond in **4** between $\{(CO)_5Cr\}$ and $\{(PCCP)Cr(CO)_5\}$. In contrast, the reactive CNCN (**1b**) forms a much stronger coordinative bond of $\Delta E = -49.6$ kcal mol^{-1}[12c] with $\{Cr(CO)_5\}$ (see Table 4). Aarnts et al.[12c] have pointed out the similarity of the coordination capabilities of CNCN and the CO ligand, which is well-known to form stable complexes. We find that the weaker Cr–PCCP interactions are mainly due to smaller overlap (Table 4). One reason is that the PCCP frontier orbitals involved are symmetrically delocalized over both ends of PCCP, whereas they are more localized on the terminal carbon atom of CNCN.

Keeping in mind that complex formation of simple phosphaalkynes P≡C–R is dominated by side-on coordination,[20] we have also briefly analyzed **6** and **7**, the side-on analogues of **3** and **4**, respectively; the results are summarized in Figure 7. Not surprisingly, the side-on complexes turn out to be more stable than their end-on analogues, but the differences are marginal: $\Delta\Delta E = -1.4$ kcal mol^{-1} for **6** relative to **3** and $\Delta\Delta E = -2.4$ kcal mol^{-1} for **7** relative to **4**.

Furthermore, we have carried out a preliminary exploration of the possibility of forming more strongly bound complexes involving dinuclear metal fragments,[20] using $[(CO)_6Co_2PCCP]$ (**8**) as a model. Complex **8** involves a tetrahedral Co_2CP unit with rather short Co–C and Co–P bonds of 2.017 and 2.275 Å and a relatively long C–P bond of 1.746 Å (see Figure 8); for comparison, the analogous Cr–C, Cr–P, and C–P bond distances in **6** are 2.394, 2.546 and 1.629 Å, respectively (see Figure 7). Note that as in **8**, a relatively long C–P bond has been experimentally observed in related dinuclear complexes of phosphaalkynes such as $[(CO)_6Co_2(t\text{-BuCP})W(CO)_5]$ (1.695(6) Å[21a]) and $[Cp_2(CO)_4Mo_2$-

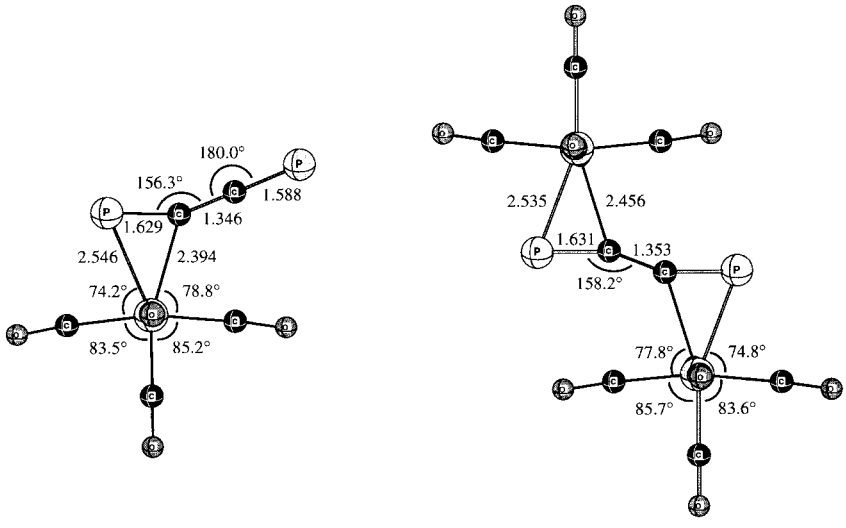

6 C_s **7** C_{2h}

6 + $Cr(CO)_5$ = −22.3 −43.9

Figure 7. BP86/TZ2P results for **6** and **7**: geometries (in Å, degrees) and electronic energies (in kcal mol^{-1}) relative to PCCP and $2\{Cr(CO)_5\}$.

0947-6539/99/0501-0172 $ 17.50+.50/0 *Chem. Eur. J.* **1999**, *5*, No. 1

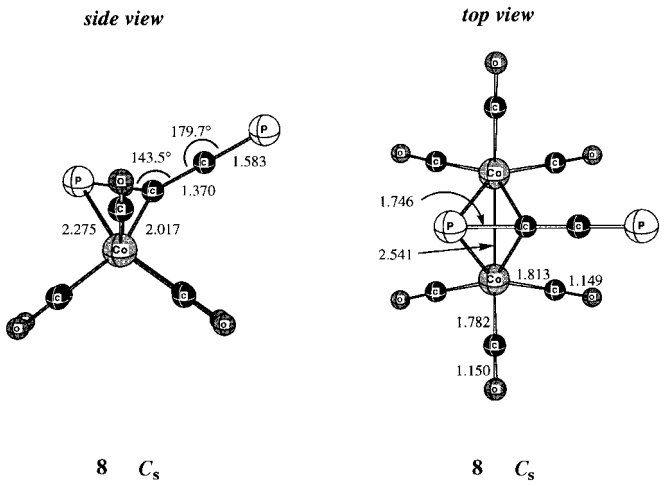

Figure 8. BP86/TZ2P geometry of **8** (in Å, degrees).

(*t*-BuCP)] (1.719(3) Å[22]). In line with this, the hypothetical dissociation of **8** into closed-shell C_{2v} {$(CO)_6Co_2$} and PCCP is rather endothermic, that is, some 76 kcal mol^{-1}. In the context of future synthetic strategies, it should be pointed out that not only complexes [$Co_2(CO)_6$(R–CP)] are known, but also those carrying an additional metal fragment bonded end-on to the phosphorus lone pair such as [$Co_2(CO)_6$(R–CP)-$W(CO)_5$];[20, 22] in analogy, complexes of the type [$Co_2(CO)_6W(CO)_5$](PC–CP)[$Co_2(CO)_6W(CO)_5$] are conceivable, which might lend considerable electronic stabilization and steric protection to PCCP (**2a**).

In conclusion, one may succeed in stabilizing the kinetically unstable **2a** in the coordination sphere of a transition metal complex. It remains to be seen if this stabilization will prove to be sufficient for isolation; possibly, mono and dinuclear transition metal complexes[20] other than those of Group 6 should also be considered.

Conclusions

1,4-Diphosphabutadiyne (PCCP, **2a**) may very well be a viable target for synthesis, as follows from our BP86/TZ2P study. The PCCP molecule turns out to be a thermodynamically stable, linear CP dimer with a 298 K carbon–carbon bond dissociation enthalpy (BDE) of 152.2 kcal mol^{-1}. The central PC–CP bond is best conceived as having partial triple bond character (i.e, P≡C–C≡P ↔ P–C≡C–P) similar to the NC–CN bond.[4i] The strength of the central bond in the CP dimers decreases in the order C–C, C–P, and P–P coupling, because of a less efficient overlap between the more diffuse phosphorus lobes of the CP σ_{SOMO}'s that provide the electron-pair bond. Note that a similar trend along the CN dimers, that is, decreasing bond strength along C–C, C–N, and N–N coupling, has a different cause, namely the increasing repulsion between the CN σ_{HOMO}'s (i.e., the N lone pairs).[4i] Compound **2a** is the global minimum of the C_2P_2 structures **2** and kinetically stable towards unimolecular isomerization.

However, we do foresee problems because of a low kinetic stability towards bimolecular reactions. This is suggested by the relatively low HOMO–LUMO gap of 2.5 eV in the π system of **2a**. For comparison, the HOMO–LUMO gap in **1a** (5.6 eV) is much higher. Thus, **2a** is likely to react with itself as soon as it is formed, giving rise to polymerization.[9]

Coordination of the terminal phosphorus atoms to a transition metal may electronically stabilize and sterically protect **2a**. Both the first and second Cr–P bond dissociation enthalpies (for 298 K) in our model complex [$(CO)_5$Cr–(PCCP)–Cr$(CO)_5$] (**4**) amount to 20 kcal mol^{-1}. These are only moderately strong coordination bonds, but the complex is presumably thermodynamically stable at ambient temperatures or below; synthetic strategies will have to be developed which take this restriction into account. Alternatively, variations in transition metal and/or auxiliary ligands may be necessary to further stabilize the system. We feel that an isolable complex of **2a** must be feasible.

Acknowledgements

F.M.B. thanks the Deutsche Forschungsgemeinschaft (DFG) for a Habilitationsstipendium.

[1] L. J. Gay-Lussac, *Ann. Chim. (Paris)* **1815**, *95*, 175.
[2] a) T. K. Brotherton, J. W. Lynn, *Chem. Rev.* **1959**, *59*, 841; b) E. Ciganek, W. J. Linn, O. W. Webster, in *The Chemistry of the Cyano Group* (Ed.: Z. Rappoport), Wiley, London, **1970**, p. 423.
[3] Experimental investigations on **1b**: a) T. van der Does, F. Bickelhaupt, *Angew. Chem.* **1988**, *100*, 998; *Angew. Chem. Int. Ed. Engl.* **1988**, *27*, 936; b) O. Grabandt, C. A. de Lange, R. A. Mooyman, T. van der Does, F. Bickelhaupt, *Chem. Phys. Lett.* **1989**, *155*, 221; c) F. Stroh, M. Winnewisser, *Chem. Phys. Lett.* **1989**, *155*, 21; d) F. Stroh, B. P. Winnewisser, M. Winnewisser, H. P. Reisenauer, G. Maier, S. J. Goede, F. Bickelhaupt, *Chem. Phys. Lett.* **1989**, *160*, 105 (erratum: *Chem. Phys. Lett.* **1989**, *162*, 253); e) K. M. T. Yamada, M. W. Markus, G. Winnewisser, W. Joentgen, R. Kock, E. Vogel, H.-J. Altenbach, *Chem. Phys. Lett.* **1989**, *160*, 113; f) M. C. L. Gerry, F. Stroh, M. Winnewisser, *J. Mol. Spectrosc.* **1990**, *140*, 147; g) A. Klesing, D. H. Sutter, F. Stroh, *J. Mol. Spectrosc.* **1991**, *148*, 149; h) F. M. Bickelhaupt, R. H. Fokkens, L. J. de Koning, N. M. M. Nibbering, E. J. Baerends, S. J. Goede, F. Bickelhaupt, *Int. J. Mass Spectrom. Ion Processes* **1991**, *103*, 157; i) S. J. Goede, F. J. J. de Kanter, F. Bickelhaupt, *J. Am. Chem. Soc.* **1991**, *113*, 6104; j) M. Winnewisser, J. G. W. Seibert, K. M. T. Yamada, *J. Mol. Spectrosc.* **1992**, *153*, 635; k) G. Maier, H. P. Reisenauer, J. Eckwert, C. Sierakowski, T. Stumpf, *Angew. Chem.* **1992**, *104*, 1287; *Angew. Chem. Int. Ed. Engl.* **1992**, *31*, 1218; l) F. Stroh, M. Winnewisser, B. P. Winnewisser, *J. Mol. Spectrosc.* **1993**, *162*, 453; m) F. Stroh, M. Winnewisser, B. P. Winnewisser, *Can. J. Phys.* **1994**, *72*, 1251; n) L. W. Jenneskens, J. W. G. Mahy, E. J. Vlietstra, S. J. Goede, F. Bickelhaupt, *J. Chem. Soc. Faraday Trans.* **1994**, *90*, 327; o) J. W. G. Seibert, M. Winnewisser, B. P. Winnewisser, F. Bickelhaupt, *J. Mol. Struct.* **1996**, *376*, 229; p) I. Weis, H. Oberhammer, S. J. Goede, P. J. K. M. Eeken, F. Bickelhaupt, unpublished results; q) R. Boese, S. J. Goede, F. Bickelhaupt, unpublished results.
[4] Theoretical investigations on **1b**: a) M. Sana, O. Leroy, *J. Mol. Struct.* **1982**, *76*, 259; b) L. S. Cederbaum, F. Tarantelli, H. G. Weikert, M. K. Scheller, H. Köppel, *Angew. Chem.* **1989**, *101*, 770; *Angew. Chem. Int. Ed. Engl.* **1989**, *28*, 761; c) M. T. Nguyen, *Chem. Phys. Lett.* **1989**, *157*, 430; d) M. K. Scheller, H. G. Weikert, L. S. Cederbaum, F. Tarantelli, *J. Electron Spectrosc. Relat. Phenom.* **1990**, *51*, 75; e) K. K. Sunil, J. H. Yates, K. D. Jordan, *Chem. Phys. Lett.* **1990**, *171*, 185; f) P. Botschwina, P. Sebald, *Chem. Phys.* **1990**, *141*, 311; g) W. B. De Almeida, A. Hinchcliffe, *J. Mol. Struct. (THEOCHEM)* **1990**, *65*, 77; h) P. Botschwina, J. Flügge, *Chem. Phys. Lett.* **1991**, *180*, 589; i) F. M. Bickelhaupt, N. M. M. Nibbering, E. M. van Wezenbeek, E. J. Baerends, *J. Phys. Chem.* **1992**, *96*, 4864; j) P. Botschwina, *Chem. Phys. Lett.* **1994**, *225*, 480; k) C. D. Sherill, H. F. Schaefer III, *J. Chem. Phys.* **1994**,

100, 8920; l) Y. H. Ding, X. R. Huang, Z. S. Li, C. C. Sun, *J. Chem. Phys.* **1998**, *108*, 2024.

[5] G. Maier, H. P. Reisenauer, J. Eckwert, C. Sierakowski, T. Stumpf, *Angew. Chem.* **1992**, *104*, 1287; *Angew. Chem. Int. Ed. Engl.* **1992**, *31*, 1218.

[6] a) K. S. Pitzer, *J. Am. Chem. Soc.* **1948**, *70*, 2140; b) R. S. Mullikan, *J. Am. Chem. Soc.* **1950**, *72*, 4493; c) H. A. Staab, *Einführung in die theoretische organische Chemie*, VCH, Weinheim, 4th ed., **1964**, p. 76; d) W. E. Dasent, *Nonexistent Compounds*, Dekker, New York, **1965**, chapter 4; e) L. D. Pettit, *Quart. Rev. Chem. Soc.* **1971**, *25*, 1; f) P. Jutzi, *Angew. Chem.* **1975**, *87*, 269; *Angew. Chem. Int. Ed. Engl.* **1975**, *14*, 232; g) L. E. Guselnikov, N. S. Nametkin, *Chem. Rev.* **1979**, *79*, 529.

[7] *Multiple Bonds and Low Coordination in Phosphorus Chemistry* (Eds.: M. Regitz, O. J. Scherer), Thieme, Stuttgart, **1990**.

[8] a) S. Smoes, C. E. Myers, J. Drowart, *Chem. Phys. Letters* **1971**, *8*, 10; b) J. Kordis, K. A. Gingerich *J. Chem. Phys.* **1973**, *58*, 5058; c) H. Bock, M. Bankmann, *Phosphorus, Sulfur, Silicon* **1990**, *53*, 167.

[9] J. Wit, M. van der Sluis, F. Bickelhaupt, unpublished results.

[10] a) J. C. Slater, *Quantum Theory of Molecules and Solids, Vol. 4*, McGraw-Hill, New York, **1974**; b) R. G. Parr, W. Yang, *Density-Functional Theory of Atoms and Molecules*, Oxford University Press, New York, **1989**; c) T. Ziegler, *Chem. Rev.* **1991**, *91*, 651; d) T. Ziegler, *Can. J. Chem.* **1995**, *73*, 743; e) E. J. Baerends, O. V. Gritsenko, *J. Phys. Chem. A* **1997**, *101*, 5383.

[11] a) B. M. Gimarc, *Molecular Structure and Bonding*, Academic Press, New York, **1979**; b) T. A. Albright, J. K. Burdett, M.-H. Whangbo, *Orbital Interactions in Chemistry*, Wiley-Interscience, New York, **1985**.

[12] a) G. Christian, H. Stolzenberg, W. P. Fehlhammer, *J. Chem. Soc. Chem. Commun.* **1982**, 184; b) G. C. Schoemaker, D. J. Stufkens, S. J. Goede, T. van der Does, F. Bickelhaupt, *J. Organomet. Chem.* **1990**, *390*, C1; c) M. P. Aarnts, D. J. Stufkens, M. Solà, E. J. Baerends, *Organometallics* **1997**, *16*, 2254.

[13] a) C. Fonseca Guerra, O. Visser, J. G. Snijders, G. te Velde, E. J. Baerends, in *Methods and Techniques for Computational Chemistry* (Eds.: E. Clementi, G. Corongiu), STEF, Cagliari, Italy, **1995**, pp. 305–395, and references therein; b) E. J. Baerends, D. E. Ellis, P. Ros, *Chem. Phys.* **1973**, *2*, 41; c) J. G. Snijders, E. J. Baerends, P. Vernooijs, *At. Nucl. Data Tables* **1982**, *26*, 483; d) P. M. Boerrigter, G. te Velde, E. J. Baerends, *Int. J. Quantum Chem.* **1988**, *33*, 87; e) L. Versluis, T. Ziegler, *J. Chem. Phys.* **1988**, *88*, 322; f) L. Fan, L. Versluis, T. Ziegler, E. J. Baerends, W. Ravenek, *Int. J. Quantum Chem. Quantum Chem. Symp.* **1988**, *S22*, 173; g) S. H. Vosko, L. Wilk, M. Nusair, *Can. J. Phys.* **1980**, *58*, 1200; h) A. D. Becke, *J. Chem. Phys.* **1986**, *84*, 4524; i) A. D. Becke, *Phys. Rev. A* **1988**, *38*, 3098; j) J. P. Perdew, *Phys. Rev. B* **1986**, *33*, 8822 (erratum: *Phys. Rev. B* **1986**, *34*, 7406); k) L. Fan, T. Ziegler, *J. Chem. Phys.* **1991**, *94*, 6057.

[14] a) T. Ziegler, A. Rauk, *Inorg. Chem.* **1979**, *18*, 1755; b) T. Ziegler, A. Rauk, *Theoret. Chim. Acta* **1977**, *46*, 1. See also, for example: c) K. Kitaura, K. Morokuma, *Int. J. Quantum. Chem.* **1976**, *10*, 325; d) K. Morokuma, *J. Chem. Phys.* **1971**, *55*, 1236.

[15] a) A. G. Maki, *J. Phys. Chem.* **1965**, *43*, 3193; b) Y. Morino, K. Kuchitsu, Y. Hori, M. Tanimoto, *Bull. Chem. Soc. Jpn.* **1968**, *41*, 2349; c) K. C. Møller, B. P. Stoicheff, *Can. J. Phys.* **1954**, *32*, 635; d) S. G. Lias, J. E. Bartmess, J. F. Liebman, J. L. Holmes, R. D. Levin, W. G. Mallard, *J. Phys. Chem. Ref. Data* **1988**, *17*, Suppl. No. 1.

[16] M. K. Scheller, L. S. Cederbaum, F. Tarantelli, *J. Am. Chem. Soc.* **1990**, *112*, 9484.

[17] The estimated BP86/TZ2P value of the asymmetric C−P stretch frequency of **4** was obtained by scaling the computed LDA/TZ2P value, through multiplying it by the ratio of the corresponding BP86/TZ2P and LDA/TZ2P values for **2a**.

[18] a) J. P. Perdew, in *Electronic Structureof Solids 1991* (Eds.: P. Ziesche, H. Eschrig), Akademie Verlag, Berlin, 1991; b) J. P. Perdew, J. A. Chevary, S. H. Vosko, K. A. Jackson, M. R. Pederson, D. J. Singh, C. Fiolhais, *Phys. Rev. B* **1992**, *46*, 6671.

[19] a) C. Lee, W. Yang, R. G. Parr, *Phys. Rev. B* **1988**, *37*, 785. See also: b) B. G. Johnson, P. M. W. Gill, J. A. Pople, *J. Chem. Phys.* **1993**, *98*, 5612; c) T. V. Russo, R. L. Martin, P. J. Hay, *J. Chem. Phys.* **1994**, *101*, 7729.

[20] a) P. Binger, *The Behaviour of λ^3,σ^1-Posphaalkynes in the Coordination Sphere of a Transition Metal*, in ref.[7], p. 90; b) J. F. Nixon, *Chem. Rev.* **1988**, *88*, 1327; c) O. J. Scherer, *Angew. Chem.* **1985**, *97*, 924; *Angew. Chem. Int. Ed. Engl.* **1985**, *24*, 924.

[21] a) J. C. T. R. Burckett-St. Laurent, P. B. Hitchcock, H. W. Kroto, M. F. Neidine, J. F. Nixon, *J. Organomet. Chem.* **1982**, *238*, C82; b) D. Seyferth, R. S. Henderson, *J. Organomet. Chem.* **1978**, *162*, C35; c) D. Seyferth, J. S. Merola, R. S. Henderson, *Organometallics* **1982**, *1*, 859.

[22] G. Becker, W. A. Herrmann, W. Kalcher, G. W. Kriechbaum, C. Pahl, C. T. Wagner, M. L. Ziegler, *Angew. Chem.* **1983**, *95*, 417; *Angew. Chem. Int. Ed. Engl.* **1983**, *22*, 413.

Received: March 26, 1998 [F1067]